Applied Catalysis B: Environmental 334 (2023) 122786

Contents lists available at ScienceDirect

Applied Catalysis B: Environmental

journal homepage: www.elsevier.com/locate/apcatb

Catalytic performance and mechanism of PTFE modified $NiCo_2O_4$ in high-salt organic wastewater treatment during wet air oxidation at ambient pressure

Liangjie Wang [a,c,d,1], Chunxiang Geng [b,1], Dawei Yu [b], Daoqing Liu [d], Hao Sun [c,d], Ke Xiao [c,*], Huazhang Zhao [d,e,**]

[a] College of Civil and Transportation Engineering, Shenzhen University, Shenzhen 518060, China
[b] College of Chemistry and Chemical Engineering, China University of Petroleum, Qingdao 266555, China
[c] Water Science and Environmental Engineering Research Center, College of Chemical and Environmental Engineering, Shenzhen University, Shenzhen 518060, China
[d] The Key Laboratory of Water and Sediment Sciences (Ministry of Education), College of Environmental Sciences and Engineering, Peking University, Beijing 100871, China
[e] Shanxi Laboratory for Yellow River, Shanxi University, Taiyuan 030006, China

ARTICLE INFO

Keywords:
Catalytic wet air oxidation
$NiCo_2O_4$
High-salt wastewater
Polytetrafluoroethylene
Mars-van Krevelen mechanism

ABSTRACT

High temperatures and high pressures restrict the application of catalytic wet air oxidation (CWAO). Thus, realizing the high performance of CWAO under ambient pressure (AP-CWAO) is attractive. In this study, hydrophobic modification by polytetrafluoroethylene (PTFE) was adopted to enhance the O_2 transfer and salts resistibility of hollow microspheres $NiCo_2O_4$ (HM-$NiCo_2O_4$), for harvesting an efficient catalyst of AP-CWAO to treat high-salt wastewater. Under ambient pressure in 10 g/L NaCl solution, PTFE modified HM-$NiCo_2O_4$ (PHM-$NiCo_2O_4$) can catalyze O_2 to realize about 70 % mineralization of bisphenol A (BPA, 100 mg/L) within 240 min at 80 ℃, while it is only about 50 % for HM-$NiCo_2O_4$. Density functional theory calculations and molecular dynamics simulations show that PTFE indeed can enhance O_2 transfer and salt resistibility of HM-$NiCo_2O_4$. HO•, $O_2^{\bullet-}$, and $^1O_2$ all contribute to the degradation of BPA in presence of O_2. These reactive oxygen species generate based on Mars-van Krevelen mechanism.

1. Introduction

Catalytic wet air oxidation (CWAO) has been widely used to treat high-salt organic wastewater due to its high efficiency when confronted with high concentrations of salts[1,2]. Although CWAO operates at lower temperatures and pressures than wet air oxidation, it still requires high temperatures (80–180 °C) and high pressures (1–5 MPa)[1,3], hence limiting its applications. CWAO that operates at ambient pressure (AP-CWAO) has attracted substantial interest because it does not require specialized equipment to withstand high temperatures and high pressures[4]. To date, it has been reported that certain metal oxide composites and Pt-loaded metal oxide composites serve as AP-CWAO catalysts[4–7]. The majority of these investigations, however, only focus on dye removal in the absence of high concentrations of salts.

Two issues need to be addressed to develop the desired AP-CWAO for high-salt organic wastewater treatment. Firstly, the degradation rates of pollutants are related to O_2 solubility to some extent[8], whereas ambient pressure and high salt concentrations result in poor O_2 solubility[9,10]. Secondly, the salts will lead to low selective degradation of organics, due to the consumption of reactive oxygen species (ROS) and occupation of catalytic active sites by inorganic ions[11]. If the affinity to O_2 and salt resistance of the catalysts are improved, their performance in AP-CWAO to treat high-salt organic wastewater will be significantly enhanced.

Inspired by 'Plastron Effect', a hydrophobic surface is helpful to catch gas from ambient water[12–14], like the hydrophobic hairy

* Corresponding author.
** Corresponding author at: The Key Laboratory of Water and Sediment Sciences (Ministry of Education), College of Environmental Sciences and Engineering, Peking University, Beijing 100871, China.
E-mail addresses: xiaoke@szu.edu.cn (K. Xiao), zhaohuazhang@pku.edu.cn (H. Zhao).
[1] These authors contributed equally to this work.

https://doi.org/10.1016/j.apcatb.2023.122786
Received 21 March 2023; Accepted 18 April 2023
Available online 6 May 2023

structure of the water spider (*Argyroneta aquatica*)[14]. Hydrophobic modification might enhance the O_2 utilization of catalysts in AP-CWAO. Besides, a hydrophobic surface is resistant to inorganic ions[15,16]. Materials are frequently endowed with hydrophobicity by using polytetrafluoroethylene (PTFE)[17,18]. PTFE possesses high stability at relatively high temperatures and under oxidation environments[19,20]. Additionally, fluoropolymers themselves have a strong affinity to oxygen[21,22]. In light of the above points, PTFE modification may improve the efficiency of the catalysts in the AP-CWAO for treating high-salt organic wastewater.

In AP-CWAO, hollow microsphere $NiCo_2O_4$ (HM-$NiCo_2O_4$) was discovered to have high catalytic performance[23]. Hence, to investigate the impact of PTFE modification on pollutant removal in AP-CWAO, particularly when dealing with high-salt organic wastewater, HM-$NiCo_2O_4$ was chosen as the catalyst in this study. The activity in solutions of various salts and reusability in high-salt conditions were used to test the catalytic performances of PTFE-modified HM-$NiCo_2O_4$ (PHM-$NiCo_2O_4$), while the catalytic mechanism was analyzed based on the formation of reactive oxygen species (ROS) and element changes under various operating conditions. More importantly, density functional theory (DFT) calculations and molecular dynamics (MD) simulations were carried out to study the role of PTFE.

2. Material and method

2.1. Chemicals

Polytetrafluoroethylene preparation (60 wt%) is from Beijing mreda Technology Co., LTD. $Co(NO_3)_2{\cdot}6\ H_2O$ (AR, 99 %), $Ni(NO_3)_2{\cdot}6\ H_2O$ (AR, 98 %), and bisphenol A (BPA, AR: 99.8 %) are the products of Shanghai Aladdin Bio-Chem Technology Co., LTD. The other chemicals, such as NaCl (AR, 99 %), Na_2SO_4 (AR, 99 %), $MgCl_2$ (AR, 99 %), and $CaCl_2$ (AR, 99 %), are all analytical reagents from Beijing Tong Guang Fine Chemicals Company.

2.2. Preparation of HM-$NiCo_2O_4$ and PTFE-modified HM-$NiCo_2O_4$

2.2.1. Preparation of HM-$NiCo_2O_4$

HM-$NiCo_2O_4$ is prepared through two steps[23–25]: 1) Precursors preparation by solvothermal method and 2) calcination of the precursors. In a typical synthesis, 2.32 g $Co(NO_3)_2{\cdot}6\ H_2O$, 1.16 g $Ni(NO_3)_2{\cdot}6\ H_2O$, and 28.8 g urea were dissolved in the mixed solution of 120 mL isopropanol and 24 mL pure water. The resulting mixture was stirred for at least 3 h to ensure the thorough dissolution of all the ingredients (the thorough dissolution is very important), and the mixture was then transferred into a 250 mL Teflon-lined stainless-steel autoclave. The autoclave was heated to 100 ℃ for keeping 2 h in an oven. After cooling to room temperature, the precipitates were collected by centrifugation, which would be washed with water and ethanol three times, respectively. Experiencing the wash and dry (105 °C, 12 h), precursors of HM-$NiCo_2O_4$ were obtained. With further calcination of the precursors at 350 °C in air for 2 h with a ramping rate of 1 °C/min, HM-$NiCo_2O_4$ would be harvested.

2.3. Preparation of PHM-$NiCo_2O_4$

PTFE-modified HM-$NiCo_2O_4$ (PHM-$NiCo_2O_4$) had a similar preparation process with HM-$NiCo_2O_4$, but before calcination, the precursors of HM-$NiCo_2O_4$ are mixed with PTFE preparation (60 wt%) with 1:10 mass ratio of PTFE to the precursors of HM-$NiCo_2O_4$, which would be further dried at 105 ℃ for 4 h to obtain PHM-$NiCo_2O_4$ (namely PHM-$NiCo_2O_4$-1:10). Besides, by changing the mass ratio of PTFE to the precursors of HM-$NiCo_2O_4$, PHM-$NiCo_2O_4$-1:2, PHM-$NiCo_2O_4$-1:5, PHM-$NiCo_2O_4$-1:8, and PHM-$NiCo_2O_4$-1:20 were prepared as well.

2.4. Characterizations

The powder X-Ray Diffraction (XRD) was performed on an X-ray diffractometer (Rigaku D/Max-Ultima+, Japan) with Cu-Kα (λ = 1.5406 Å) radiation to obtain crystallographic information of the materials. Scanning electron microscope (SEM, Zeiss Supra55, Germany) and transmission electron microscope (TEM, FEI Tecnai G2 F30, America) were used to observe the morphologies of the materials. The element compositions of the materials were measured by X-ray photoelectron spectra (XPS) from AXIS Supra system (Kratos, England) with a monochromatic Al Kα radiation source. Autosorb-iQ automated gas sorption analyzer (Quantachrome, USA) was used to analyze the Brunauer-Emmett-Teller (BET) specific surface areas of the materials. Contact angles of the materials were measured by Surface Analyser (LAUDA Scientific, Germany). The Fourier-transformed infrared (FT-IR) spectra were obtained by a Nicolet iS50 FT-IR spectrometer (Thermo Scientific, USA) using KBr disc method. Electron paramagnetic resonance (EPR) tests were adapted to detect the reactive oxygen species by a JES-FA300 (JEOL, Japan) spectrometer, using 5,5-dimethyl-1-pyrroline N-oxide (DMPO) as the spin-trapping agent of HO• and $O_2^{\bullet-}$, and 2,2,6,6-Tetramethylpiperidine (TEMP) as the spin-trapping agent of $^1O_2$.

2.5. Degradation experiments

In the actual phenolic wastewaters (such as petrochemicals: 2.8–1220 mg/L, petroleum oil refineries: 6–500 mg/L, and coke oven plants (28–1200 mg/L), the concentrations of phenolic compounds vary from several to hundreds mg/L[26,27]. In this study, a moderate concentration of BPA (100 mg/L) was selected for the degradation experiments.

The apparatus used for pollutants degradation is shown in Fig. 3a. Firstly, 80 mL BPA solution (100 mg/L) and a certain mass of inorganic salt (solid) were put into a 250 mL round bottom flask with three necks, and the mixture was stirred until dissolution. Secondly, the tap was turned on to provide constant cold water for reflux condensation of the BPA solution, and the flask was heated to the target temperature by water bath. Thirdly, the catalyst was added into the BPA solution with immediately starting the magnetic stirring and bubbling oxygen into the BPA solutions at a rate of 150 mL/min, and the start of bubbling oxygen was deemed to be the start of the degradation. At last, 2 mL sample would be collected at the set time and filtered by 0.22 μm polyethersulfone membrane filters, and the filtrate would be used for further analysis. Before the detection of TOC, the samples need to be diluted to make the concentration of TOC less than 10 mg/L (upper limit of the standard curve). For each degradation experiment, the background value (namely, without addition of BPA) of TOC needs to be tested. In the calculation of the TOC removal rate, the background value will be subtracted.

In the reusability tests, the catalysts would be recycled by a centrifuge. Before they are reused, the catalysts would undergo two kinds of treatment methods: without wash and with wash. In the mode without wash, the catalysts were reused after drying at 60 ℃. As for wash mode, before drying, the catalysts were washed with deionized water, ethanol, and deionized water in sequence.

2.6. DFT calculations and MD simulations

DFT calculations were carried out to study the interactions between catalysts and inorganic ions (or O_2), in which ORCA 5.0.3[28] and Multiwfn 3.8 software[29] were used. The influence of PTFE on the distribution of O_2 was simulated by MD using LAMMPS software package[30]. Detailed information of DFT calculations and MD simulations can be found in Supporting information (Text S1 and Text S2).

3. Results and discussions

3.1. Characteristics of HM-$NiCo_2O_4$ and PHM-$NiCo_2O_4$

The obtained HM-$NiCo_2O_4$ (Fig. S2a) and PHM-$NiCo_2O_4$ (Fig. 1a) are both hollow microspheres with many nanorods radially formed on the surface (Fig. 1b and c), which are similar to previous studies[23,24,31]. The precursor of HM-$NiCo_2O_4$ has a morphology similar to HM-$NiCo_2O_4$ (Fig. S2b). When compared to the known standard in JCPDS file (No. 20–0781)[23], the catalysts prepared with or without PTFE are both $NiCo_2O_4$ (Fig. 2a), indicating that $NiCo_2O_4$ was successfully prepared and that PTFE had no influence on $NiCo_2O_4$ formation. XPS analysis (Fig. 2b and Table S1), energy-dispersive X-ray (EDX) mapping (Fig. S3a-d) and FT-IR spectra (Fig. S3f) show that PTFE had been combined into $NiCo_2O_4$ in PHM-$NiCo_2O_4$, because of the emergence of F element and C-F bond vibrations. However, no XRD peaks of PTFE (JCPDS file: No. 54–1595) were found. Pure PTFE has a sharp peak at 18.1° (2θ) whether or not being treated under 350 ℃ (Fig. S3e), proving the thermal stability of PTFE. In the XRD pattern of PHM-$NiCo_2O_4$ (namely, PHM-$NiCo_2O_4$-1:10), no peak of PTFE existed. However, peaks at about 1154 and 1221 cm^{-1} (C-F bond vibrations) in FT-IR analysis were found for PHM-$NiCo_2O_4$ (Fig. S3f). Besides, in PHM-$NiCo_2O_4$-1:2 (mass ratio: PTFE/$NiCo_2O_4$ = 1:2), the XRD peak of PTFE was found but with a low intensity (Fig. S3e), indicating that PTFE in the composite indeed has crystal structure. Thus, the low content of PTFE is very likely to be the reason for no PTFE XRD peak in PHM-$NiCo_2O_4$.

The lattice distance of (1 0 0) surface of PTFE is 0.49 nm, which is larger than these lattice distances of all surfaces of $NiCo_2O_4$ displayed in the XRD pattern. Thus, 0.49 nm lattice fringes can be used to distinguish $NiCo_2O_4$ from PTFE. Based on this point, Fig. 1d shows that PTFE and $NiCo_2O_4$ present intergrowth structure, and a partially enlarged detail is shown in Fig. 1e. Lattice fringes of 0.25 nm and 0.49 nm in Fig. 1e correspond to the (3 1 1) surface of $NiCo_2O_4$ and (1 0 0) surface of PTFE, respectively. Furthermore, the PTFE/HM-$NiCo_2O_4$ ratio seems to be higher than 1:10 in Fig. 1d. Because $NiCo_2O_4$ has hollow structures, PTFE should be more likely to distribute on the external surface, resulting in a higher PTFE ratio on external surface.

HM-$NiCo_2O_4$ and PHM-$NiCo_2O_4$ have BET surface areas of 55.6 and 73.7 m^2/g, respectively, and their average pore sizes are 21.1 and 21.5 nm, respectively. Both of their hysteresis loops are H3 type (Fig. 2c and d) which correspond to slit-shaped pores[32,33]. The slit-shaped pores should be related to the numerous nanorods on the surface of the catalyst. The contact angles of HM-$NiCo_2O_4$ are 22.28° and 22.28°, whereas they are 44.80° and 33.66° for PHM-$NiCo_2O_4$ (Fig. 2e and f), demonstrating that PTFE modification improved the hydrophobicity of $NiCo_2O_4$. PHM-$NiCo_2O_4$ has larger contact angles, but they are still less than 90°, indicating that it is hydrophilic. However, the intergrowth structure of PTFE and $NiCo_2O_4$ can result in local hydrophobicity, which also can improve the affinity of PHM-$NiCo_2O_4$ to O_2 and its resistance to salts.

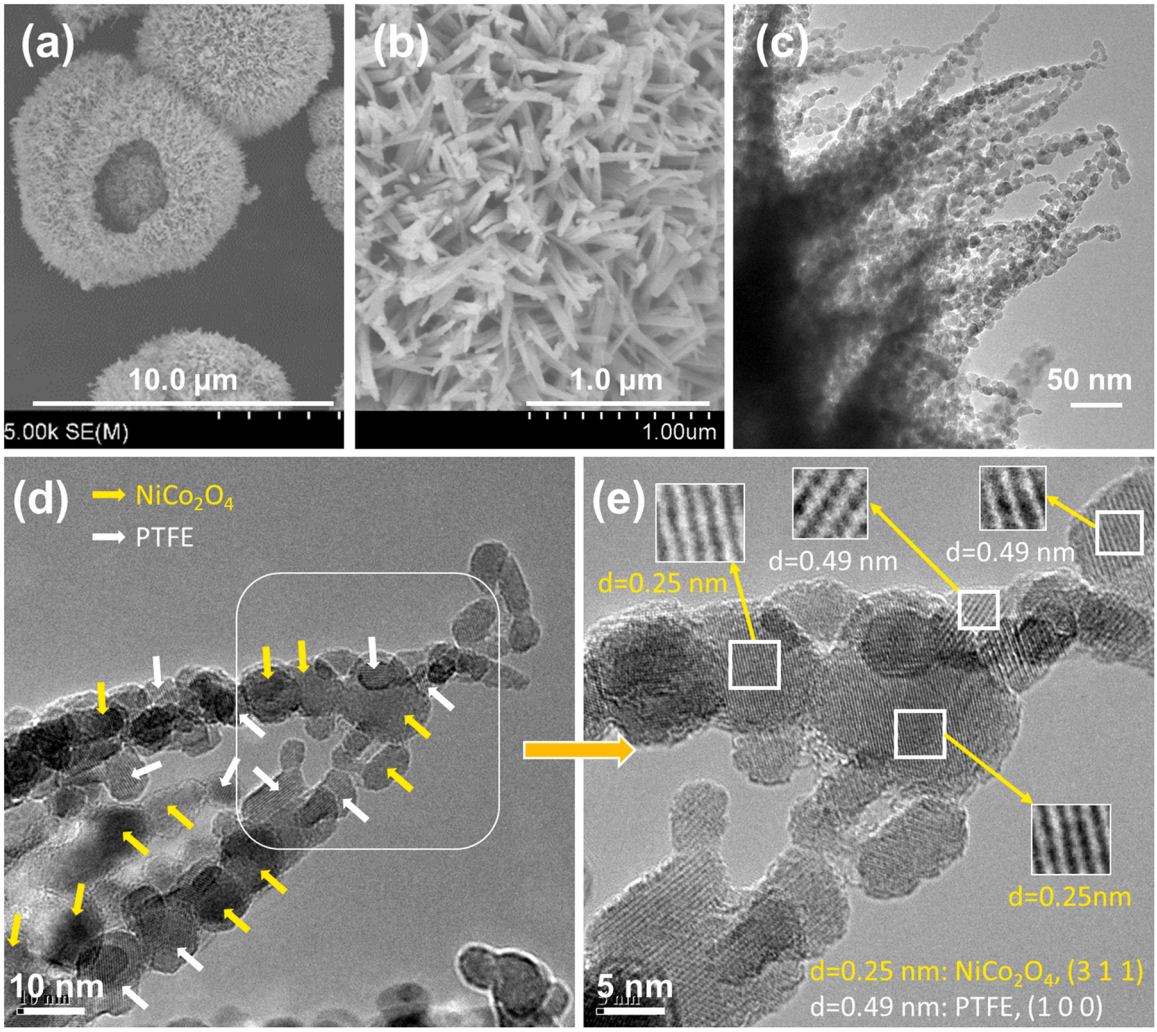

Fig. 1. SEM (a and b) and TEM (c-e) of PHM-$NiCo_2O_4$ (The identification of PTFE and $NiCo_2O_4$ in d and e are both based on lattice distance).

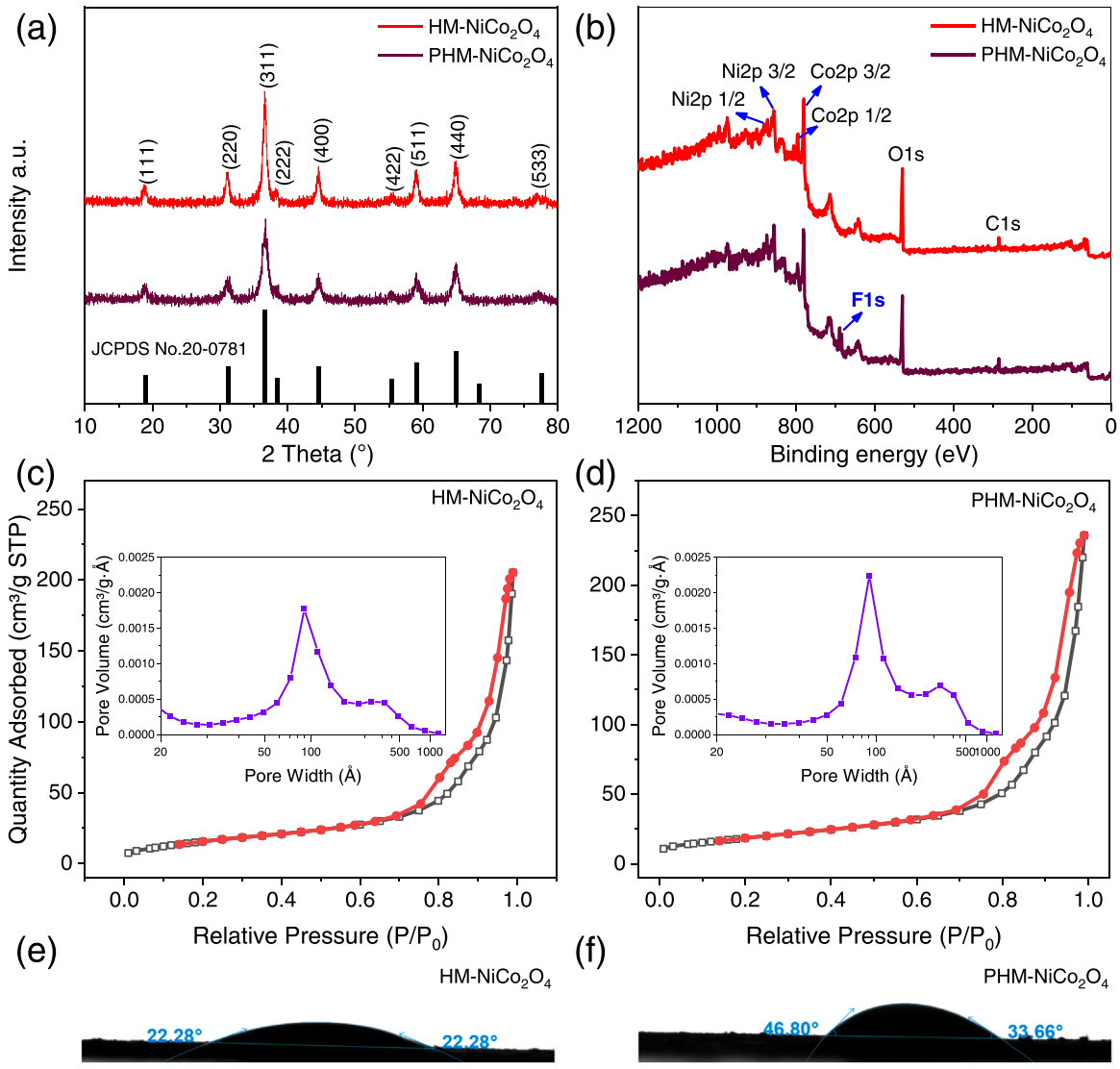

Fig. 2. XRD patterns (a), XPS full-scan spectra (b), N_2 sorption−desorption isotherms (c and d) and contact angles (e and f) of HM-$NiCo_2O_4$ and PHM-$NiCo_2O_4$.

3.2. Catalytic performance of PHM-$NiCo_2O_4$

3.2.1. The performance of PHM-$NiCo_2O_4$

3.2.1.1. The enhancement of PTFE in TOC removal. In the absence of NaCl, HM-$NiCo_2O_4$ and PHM-$NiCo_2O_4$ removed 71.5 % and 79.8 % of total organic carbon (TOC) within 240 min, respectively (Fig. 3b). Generally, hydrophobic modification can result in higher adsorption capacity to some organics[34,35]. As a result, it is easy to misunderstand that PTFE modification improves the adsorption instead of degradation of BPA. However, PTFE has the property of both strong hydrophobicity and lipophobicity. The lipophobicity makes PTFE has no adsorption ability to BPA (Fig. 3d). Thus, PTFE modification would play a negative role in BPA adsorption. Under N_2 atmosphere, PHM-$NiCo_2O_4$ has lower ability to remove TOC than HM-$NiCo_2O_4$ in the absence of NaCl (Fig. 3b), indicating that the PTFE modification enhanced BPA degradation instead of BPA adsorption. Within the first 60 min under O_2 atmosphere, PHM-$NiCo_2O_4$ has lower TOC removal rate than HM-$NiCo_2O_4$ in the absence of NaCl. It might be that at the initial period, adsorption and lattice oxygen contribute a lot to TOC removal. PHM-$NiCo_2O_4$ has stronger ability to contact O_2 than HM-$NiCo_2O_4$, thus, after the consumption of lattice oxygen and adsorption capacity in the first 60 min, the TOC removal rate of PHM-$NiCo_2O_4$ exceeds HM-$NiCo_2O_4$.

In the presence of 10 g/L NaCl, the TOC removal rate of HM-$NiCo_2O_4$ lost about 20 %, but it was only 10 % for PHM-$NiCo_2O_4$ (Fig. 3b), indicating that PTFE modification can enhance the salt resistance. Noting that in the presence of 10 g/L NaCl, HM-$NiCo_2O_4$ has a much lower TOC removal rate than PHM-$NiCo_2O_4$ within the first 60 min in the presence of NaCl, which is inverse to the case in absence of 10 g/L NaCl. This phenomenon implies that NaCl not only inhibits the degradation but also the adsorption of BPA. In other words, PTFE modification is helpful to the adsorption of BPA in the presence of 10 g/L NaCl. It needs to note that this enhancement is not from the direct adsorption of BPA by PTFE, but it is because PTFE modification hinders the interaction between the catalyst and NaCl.

Due to the short lifetimes of ROS, they mainly distribute on the surface of the catalyst. Thus, the adsorption of BPA on the surface of the catalyst is crucial for its degradation. However, based on the above discussion, it is still unclear whether the enhancement of TOC removal in the presence of 10 g/L NaCl is owing to only adsorption or degradation after the adsorption. If adsorption contributes a lot to BPA removal, the ability of the catalyst to remove BPA should have a significant decrease at the second use without cleaning the catalyst surface, because most of the adsorption sites have been occupied in the first use. However, undergoing three cycles without washing catalysts, the TOC removal rate only decreased by about 15 % (Fig. S6a), indicating that

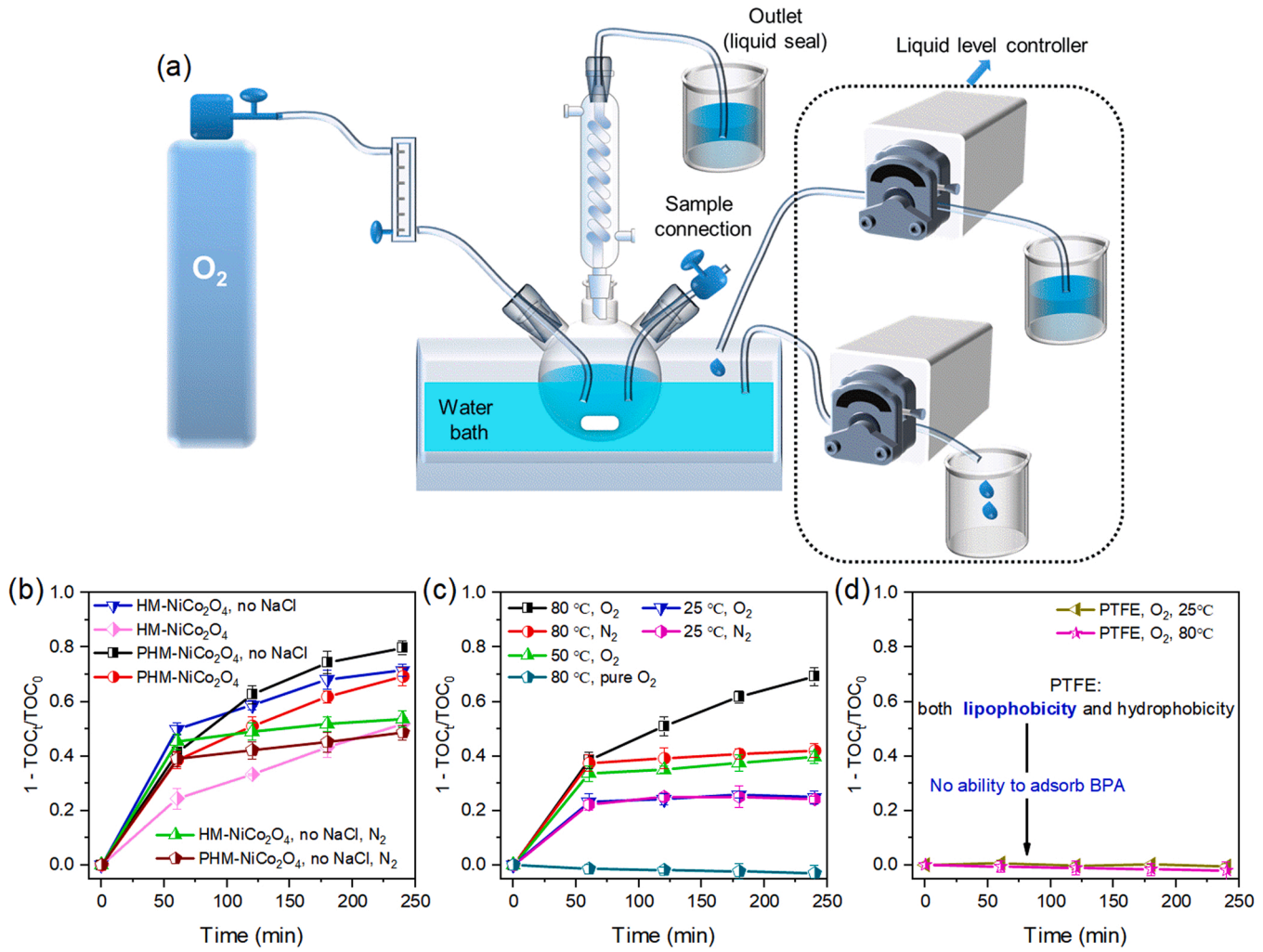

Fig. 3. The apparatus used in degradation experiments (a), the enhancement of BPA removal by PTFE modification (b), the removal of BPA under different conditions in the presence of 10 g/L NaCl (c), and the removal of BPA by only PTFE (d) ([catalyst] = 2 g/L, [O_2 or N_2] = 150 mL/min, [NaCl] = 10 g/L, $[BPA]_0$ = 100 mg/L, initial pH: unadjustment).

the BPA was degraded after adsorption.

According to the performance comparison of PHM-$NiCo_2O_4$ and HM-$NiCo_2O_4$ in the absence or presence of 10 g/L NaCl, PTFE modification should have improved both O_2 transfer and salt resistibility of the catalysts. The related mechanisms will be discussed in the 3.2.2 section. PTFE modification improved about 18% removal of TOC in the solution of 10 g/L NaCl, while it is about 8% in the case without NaCl. Thus, in the solution of 10 g/L NaCl, the enhancement of PTFE modification on O_2 transfer and salt resistibility contribute 8% and 10% increase in TOC removal, respectively.

3.2.1.2. The influence of PTFE ratio, temperature, and pH on BPA removal. $NiCo_2O_4$ plays the role to degrade BPA, while PTFE can enhance the O_2 transfer and salt resistance, but PTFE cannot directly activate O_2. Thus it needs a suitable ratio of $NiCo_2O_4$ and PTFE to obtain the best catalytic performance. Other PHM-$NiCo_2O_4$ with different PTFE ratios (PTFE/HM-$NiCo_2O_4$ = 1:2, 1:5, 1:8, and 1:20, respectively) were prepared as well. As shown in Fig. S4a, with a 1:10 ratio, PHM-$NiCo_2O_4$ performed best, which was used for further experiments.

The temperature has a significant influence on the performance of PHM-$NiCo_2O_4$. The TOC removal rates were 69.2 %, 39.6 %, and 24.8 % at 80 ℃, 50 ℃, and 25 ℃ for 240 min treatment, respectively (Fig. 3c). At 25 ℃, the removal of TOC should be mainly owing to adsorption but not degradation, because TOC removal at this temperature has little differences under O_2 an N_2 atmosphere. Even without O_2, PHM-$NiCo_2O_4$ can remove 39.6 % of TOC at 80 ℃. Both adsorption and degradation contribute the removal of TOC under N_2 atmosphere at 80 ℃, because HO• was found in this condition (Fig. 8). In addition, in the presence of O_2 but without catalyst, there is no TOC removal (Fig. 3c), and in this condition, even for BPA itself, no removal was found (Fig. S5), indicating the good catalytic activity of PHM-$NiCo_2O_4$. The pH of 100 mg/L BPA solution is about 6.4. From pH 5–9, pH has no obvious influence on TOC removal (Fig. S4b).

3.2.2. *The enhancement mechanism of PTFE*

3.2.2.1. The enhancement of PTFE on O_2 transfer. The high efficiency of BPA removal needs O_2 (Fig. 3c). The surface of $NiCo_2O_4$ is hydrophilic, which is hard to contact the O_2 bubbles. As a result, the utilization of O_2 by $NiCo_2O_4$ needs gas(O_2 bubbles)-liquid(dissolved O_2)-solid (adsorbed O_2) transfer. However, the low solubility of O_2 lead to low efficiency of O_2 transfer in the gas-liquid interface. As known, the hydrophobic surface is helpful to contact the gas in water[12–14]. Thus, the local hydrophobicity caused by PTFE modification may improve the O_2 transfer.

Although compared with MD simulations, DFT calculation is more precise, the interaction between catalyst and gas cannot be calculated by DFT calculation. Thus, MD simulations were carried out to verify whether PTFE enhanced O_2 transfer or not. As shown in Fig. 1e and Figs. 2a, (3 1 1) is the most exposed surface of PHM-$NiCo_2O_4$. Besides, compared with Ni, Co and O played more important roles, which were

proved in Section 3.3.2. Thus, the MD simulations were carried out based on two kinds of models: Co atoms exposure on the (3 1 1) surface (Fig. 4b0) and O atoms exposure on the (3 1 1) surface (Fig. 4c0). In the left part of Fig. 4b1 and c1, namely the part with PTFE modification, nanobubbles formed, due to the hydrophobicity of PTFE. According to Fig. 4b2 and c2, in the part of PTFE modification, there is more O_2 distribution. The O_2 distributions along *z* direction (Fig. 4b3, b4, c3, and c4) also show that more O_2 distribute on the surface of PTFE, indicating that the PTFE modification is helpful to capture O_2. Although the distribution of O_2 confirms that O_2 is prone to distribution on the surface of PTFE, the most important point is the formation of nanobubbles in the PTFE part. In the original model, there are no nanobubbles, but it formed after 20 ns MD simulations. This phenomenon shows that PTFE modification can significantly improve the ability of the catalyst to contact the gas in water, which is helpful to use the O_2 in gas phases. Besides, the existence of nanobubbles will occupy some space in the PTFE part. Thus, the number of O_2 should become less in the PTFE part. However, even with nanobubbles, the number of O_2 in the PTFE part is still higher than in another part (Fig. 4b3, b4, c3, and c4), indicating that PTFE has a high ability to capture O_2.

The distributions of O_2 are calculated based on the statistics in three-dimensional space, while Fig. 4b1 and c1 are the two-dimensional cross section. As a result, it is not easy to fully observe the final results only based on Fig. 4b1 and c1. Thus, the final trajectory files (.mol2 file) of these two systems are provided in the electronic supplementary documents, which can be opened by VMD software.

Noting that, the accumulation of O_2 on the surface of PTFE is caused by the hydrophobic effect rather than the traditional adsorption effect. If PTFE had strong ability to bind O_2, the O_2 is hard to be transferred from the PTFE surface to the $NiCo_2O_4$ surface, not to mention the utilization of O_2 by $NiCo_2O_4$. This mechanism has been reported in the previous study, namely, perfluorocarbons cannot bind gases chemically[22]. Our DFT calculations (Fig. 5) show that the interaction between O_2 and PTFE is weak as well, but it is relatively strong between O_2 and $NiCo_2O_4$, which means that $NiCo_2O_4$ can grab O_2 from the PTFE surface, like the way in Fig. 6A. In the interface area, the blue mark part in Fig. 4b2 and c2, there was a high concentration of O_2, indicating that the A pathway showed in Fig. 6 is reasonable.

3.2.2.2. The enhancement of PTFE on salts resistibility. According to DFT calculations (Fig. 5), the adsorption energy between Cl^- and $NiCo_2O_4$ is significantly larger than that between Cl^- and PTFE. As shown in Fig. 5, there is a strong electrostatic interaction between Cl^- and $NiCo_2O_4$, but it is weak dispersion interaction between Cl^- and PTFE. The interactions between PTFE and other inorganic ions (Na^+, SO_4^{2-}, Mg^{2+}, and Ca^{2+}) are weak as well (Fig. 5). Obviously, the enhanced salt tolerance of PHM-$NiCo_2O_4$ is from PTFE modification (the B pathway in Fig. 6).

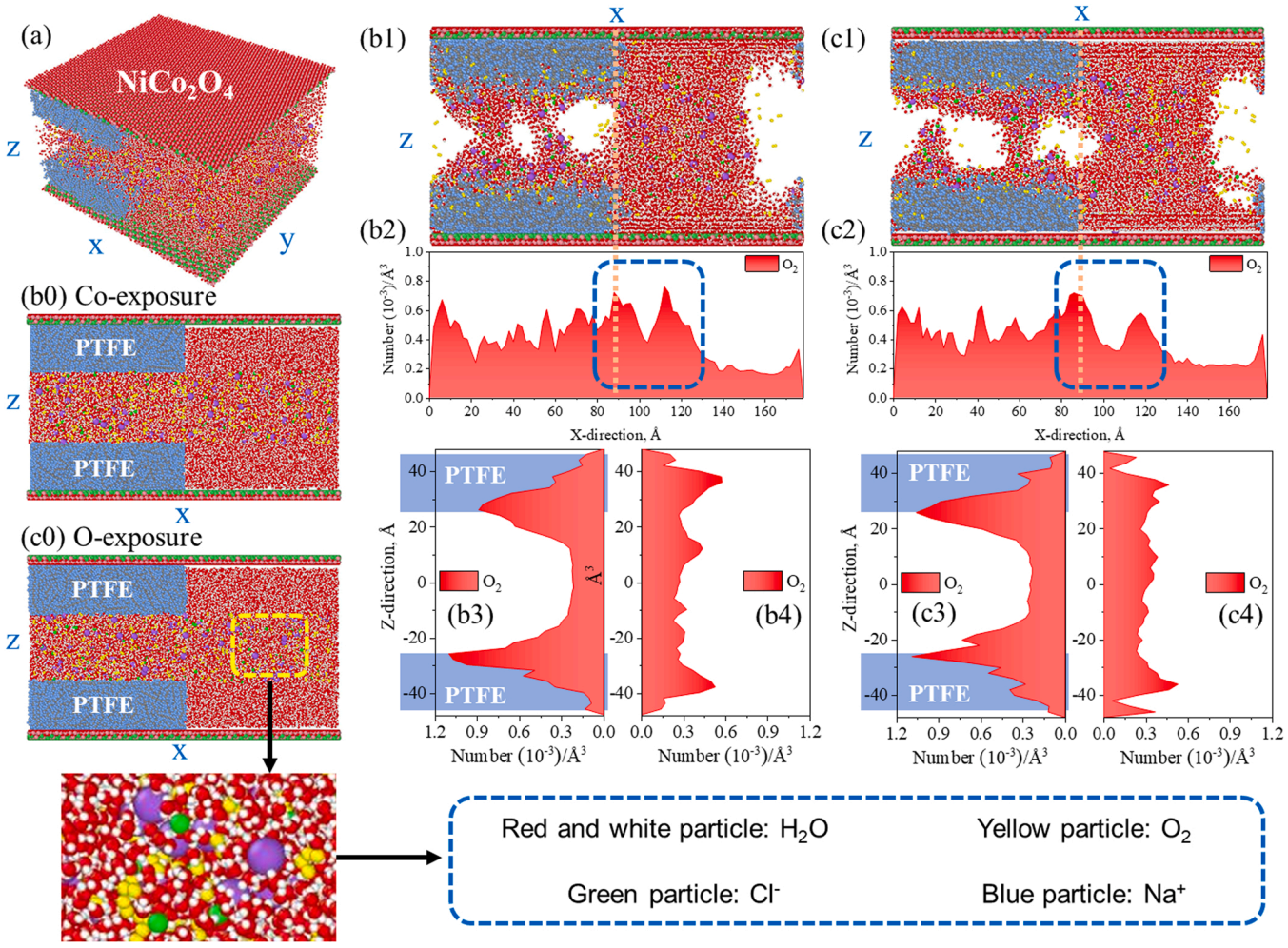

Fig. 4. MD simulations of O_2 distribution on the surface of PTFE and $NiCo_2O_4$: (a) three-dimensional diagram of the PHM-$NiCo_2O_4$ model used in the MD simulations; (b0 and b1) the *x*-*z* cross section of PHM-$NiCo_2O_4$ with Co atoms exposure before and after MD simulations, (b2) the O_2 distribution along *x* direction, (b3) the O_2 distribution along *z* direction in the left part (PTFE part), (b4) the O_2 distribution along *z* direction in the right part (no PTFE part); (c0 and c1) the *x*-*z* cross section of PHM-$NiCo_2O_4$ with O atoms exposure before and after MD simulations, (c2) the O_2 distribution along *x* direction, (c3) the O_2 distribution along *z* direction in the left part (PTFE part), (c4) the O_2 distribution along *z* direction in the right part (no PTFE part).

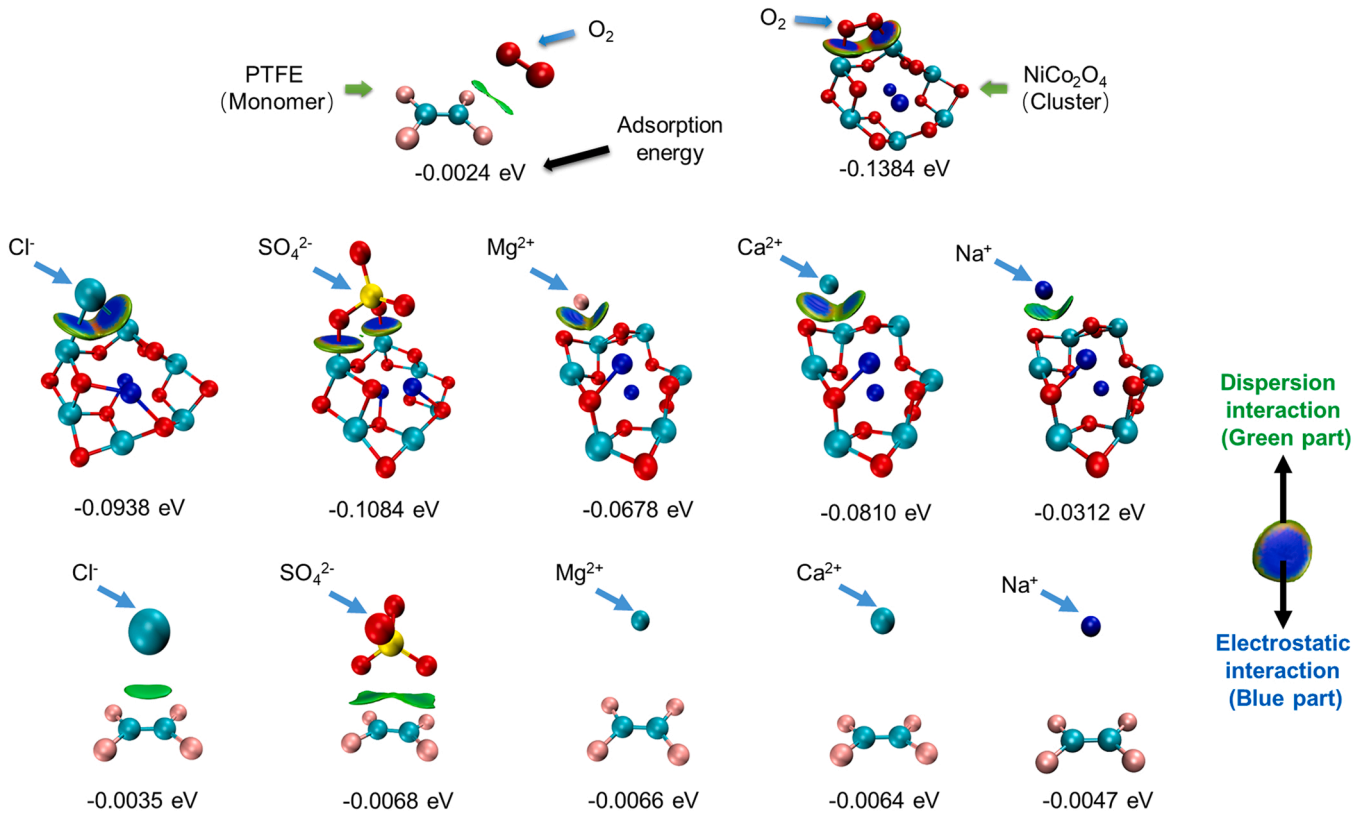

Fig. 5. DFT calculation results of the weak interaction and adsorption energy between inorganic ions and materials.

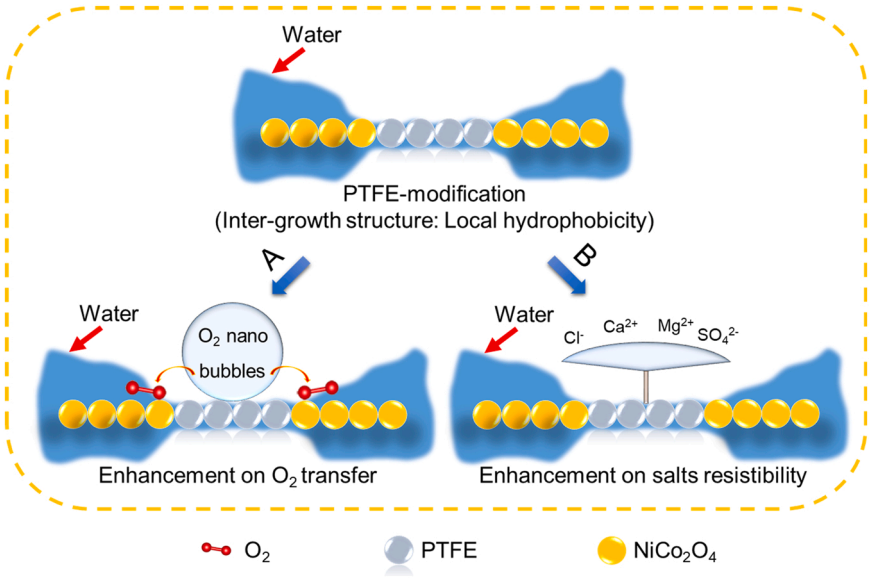

Fig. 6. Schematic diagram of the enhancement of PTFE modification on catalytic performance of HM-$NiCo_2O_4$.

3.2.3. The influence of inorganic ions on the performance of PHM-$NiCo_2O_4$

In high-salt organic wastewater, there are various kinds of inorganic ions. These inorganic ions may have a negative effect on the catalytic performance of PHM-$NiCo_2O_4$. As shown in Fig. 7, as the concentration of these organic ions rose from 0 g/L to 10 g/L, NaCl and $MgCl_2$ lead to about 15 % decrease of TOC removal rate within 480 min degradation, while Na_2SO_4 and $CaCl_2$ result in about 40% decrease. To compare the influence of inorganic anions (Cl^- and SO_4^{2-}), NaCl and Na_2SO_4 were selected. Na^+ might influence the TOC removal as well. With a concentration of 10 g/L, the molar concentrations of NaCl and Na_2SO_4 are 0.171 M and 0.070 M, respectively. Even with a lower molar concentration of Na^+ and SO_4^{2-} (vs Cl^-), Na_2SO_4 has much higher ability to suppress the TOC removal than NaCl, indicating that the inhibition effect is mainly from SO_4^{2-} instead of Na^+. $MgCl_2$ and $CaCl_2$ were used to compare the influence of Mg^{2+} and Ca^{2+}. With a concentration of 10 g/L, the molar concentrations of $MgCl_2$ and $CaCl_2$ are 0.105 M and 0.090 M, respectively. The molar concentrations of $MgCl_2$ and $CaCl_2$ are similar, but $CaCl_2$ has much stronger ability to inhibit TOC removal than

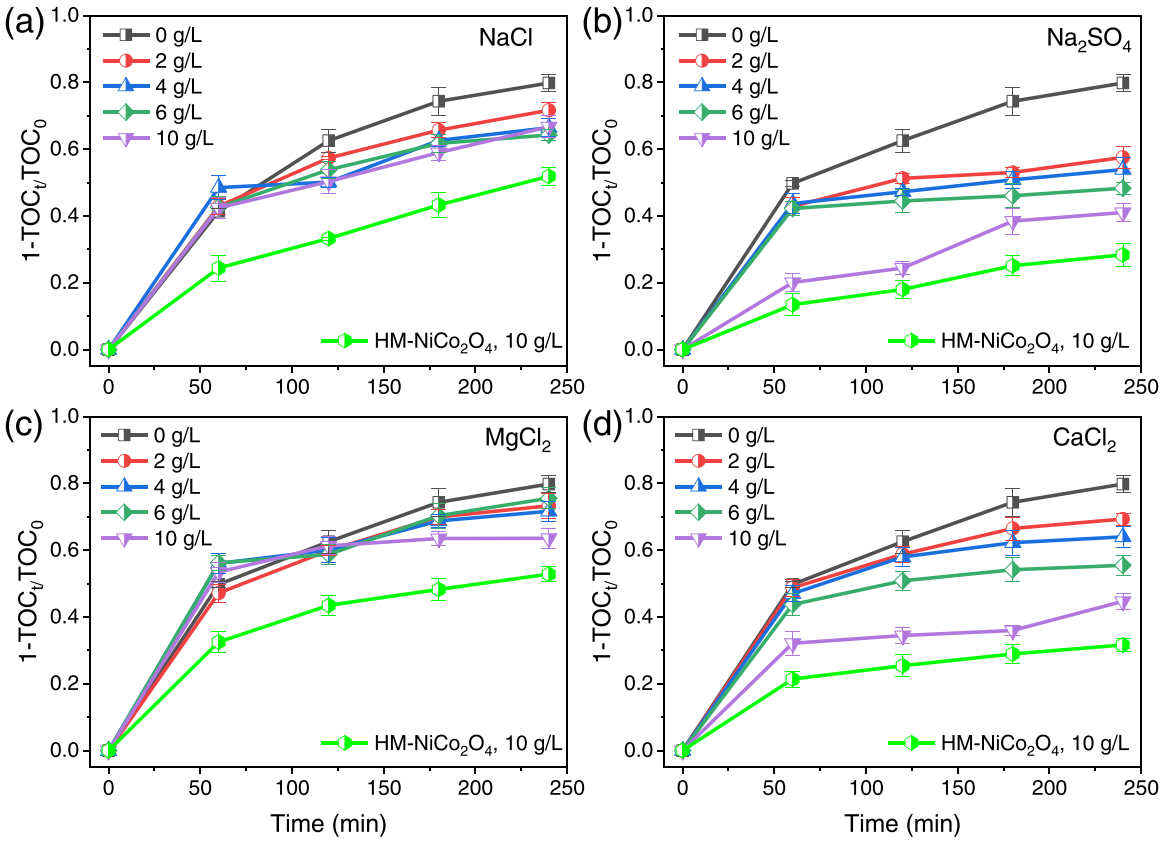

Fig. 7. The influence of NaCl, Na_2SO_4, $MgCl_2$ and $CaCl_2$ on the performance of PHM-$NiCo_2O_4$ to remove BPA ([catalyst] = 2 g/L, $[O_2]$ = 150 mL/min, $[BPA]_0$ = 100 mg/L, initial pH: unadjustment).

$MgCl_2$, demonstrating that Ca^{2+} plays a more important role than Cl^- in the inhibition of TOC removal. As for NaCl, the inhibition effect should be mainly from Cl^-, because DFT calculation shows that the adsorption energy between Na^+ and $NiCo_2O_4$ is only − 0.0312 eV, which is much lower than that between Cl^- and $NiCo_2O_4$ (−0.0938 eV) (Fig. 5).

Although compared with HM-$NiCo_2O_4$, PHM-$NiCo_2O_4$ has better performance facing these four inorganic ions (Fig. 7), PHM-$NiCo_2O_4$ is not suitable to treat high-salt organic wastewaters with SO_4^{2-} and Ca^{2+} as the main inorganic components, because the high concentration of SO_4^{2-} and Ca^{2+} can lead to significant decrease of TOC removal.

The inhibition effects of these inorganic ions in TOC removal can be caused by both their occupation of catalytic sites and consumption of ROS. Cl^- and SO_4^{2-} can react with HO• (2.7 V) to form $Cl^•$ (2.4 V) and $SO_4^{•-}$ (2.5–3.1 V), respectively[36–39]. The redox potential of $Cl^•$ is slightly lower than that of HO•, therefore, the TOC removal rate only lost about 10% in a solution of 10 g/L NaCl. Although the redox potential of $SO_4^{•-}$ is similar to HO•, SO_4^{2-} may occupy some active sites of catalyst[11]. SO_4^{2-} own higher interaction with the catalyst than Cl^- (Fig. 5). In addition, the reaction rate between HO• and BPA is higher than that between $SO_4^{•-}$ and BPA[40]. As a result, SO_4^{2-} had a relatively higher inhibition effect on TOC removal. Compared with Mg^{2+}, Ca^{2+} has stronger adsorption energy with catalyst, and as a result, the inhibition of Ca^{2+} on TOC removal is more serious.

3.2.4. The reusability and application of PHM-$NiCo_2O_4$

To assess the reusability of PHM-$NiCo_2O_4$, two operational modes were employed, namely, unwashed and washed modes (Fig. S6a). Furthermore, due to that complete degradation of bisphenol A (BPA) was achieved within 480 min (Fig. S7), the degradation of pollutants was evaluated for 480 min in each cycle during the reusability tests. Under the unwashed mode, PHM-$NiCo_2O_4$ exhibited 64.6 % of TOC removal in the third cycle, but the TOC removal rate significantly declined to 36.5% in the fourth cycle. The TOC removal rate decreased by only 8 % over four cycles in the washed mode. Despite the partial collapse of PHM-$NiCo_2O_4$ after use (Fig. S8), the levels of leached Co^{2+} and Ni^{2+} were both less than 1.0 mg/L in each cycle under the unwashed mode (Table S2). Notably, the leached Co^{2+} and Ni^{2+} did not contribute to the removal of BPA (Fig. S6b), indicating the excellent reusability of PHM-$NiCo_2O_4$. To validate the applicability of PHM-$NiCo_2O_4$, humic acid (HA), bisphenol S (BPS), carbamazepine (CBZ), and 4-chlorophenol (4-CP) were chosen as the target pollutants. The removal rates of TOC for all these pollutants exceeded 60% (Fig. S4c).

3.3. Catalytic mechanism of PHM-$NiCo_2O_4$

3.3.1. Identification of ROS

To determine the key ROS, EPR tests were conducted. Strong EPR signals were observed for HO•, $O_2^{•-}$, and $^1O_2$ in the presence of O_2 (Fig. 8a1-c1). BPA addition diminished the intensity of the EPR signals of HO•, $O_2^{•-}$, and $^1O_2$ (Fig. 8a2-c2), indicating that these ROS all contributed to the degradation of BPA. In the absence of O_2, only the EPR signal of HO• was detected (Fig. 8a3-c3), indicating that the specific O species of $NiCo_2O_4$ are converted into HO•. The absence of $O_2^{•-}$ and $^1O_2$ under N_2 atmosphere proves that $O_2^{•-}$ and $^1O_2$ are produced from the interaction between $NiCo_2O_4$ and O_2, or between HO• and O_2. The EPR signal intensity of HO• under O_2 is much higher than that under N_2, demonstrating that the consumed O species of $NiCo_2O_4$ for HO• generation can be compensated by O_2. Due to the constant production of ROS in the presence of O_2, the EPR signal intensities of these ROS increased dramatically from 1 to 30 min (Fig. S9 - Fig. S11).

3.3.2. Active sites of PHM-$NiCo_2O_4$

For AP-CWAO, the mechanisms of ROS formation are grouped into four categories: Hopping conduction model (HC) mechanism, surface

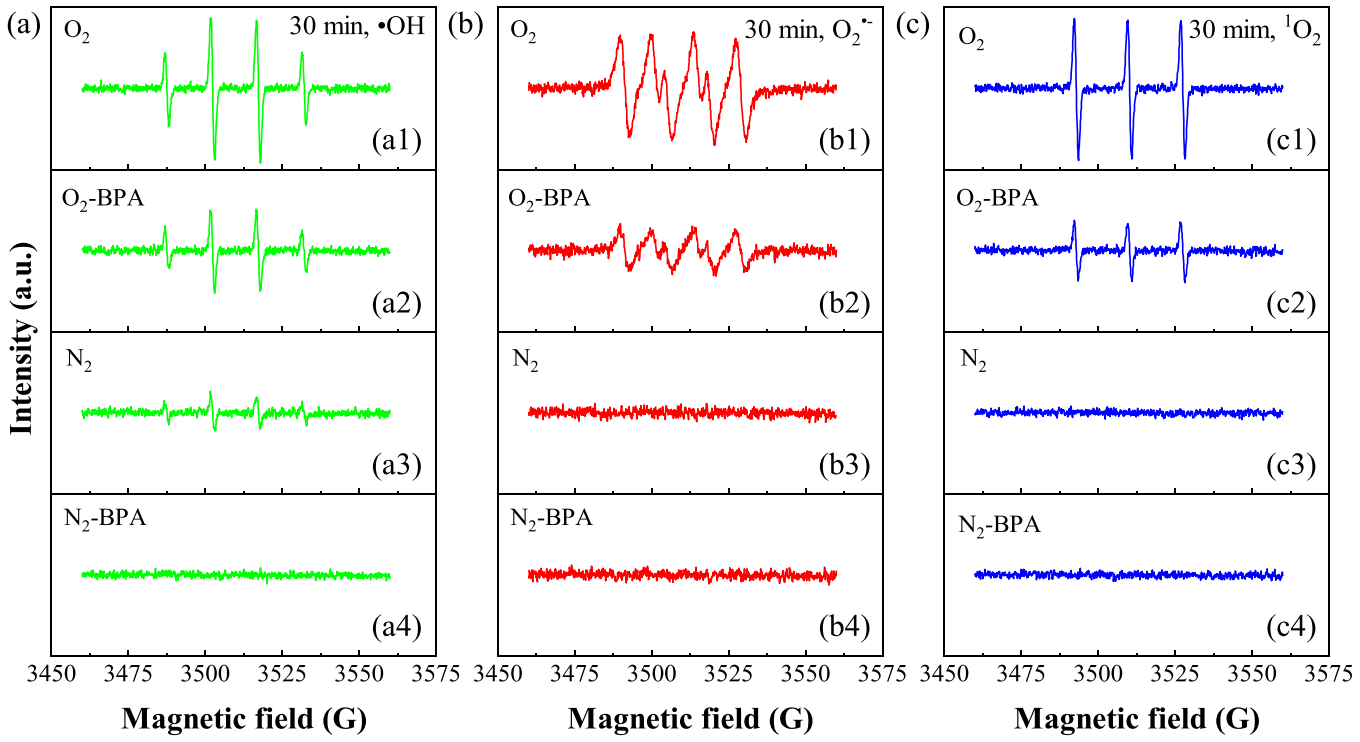

Fig. 8. EPR spectra of DMPO-OH (a), DMPO-OOH (b) and TEMP-$^1O_2$ (c) without and with BPA in the presence of O_2 or N_2 ([catalyst] = 2 g/L, $[BPA]_0$ = 100 mg/L, [temperature] = 80 ℃).

electron-transfer (SET) mechanism, free radical chain autoxidation (FRCAO) mechanism and Mars-van Krevelen (MVK) mechanism[4]. In the HC process, free electrons and positive holes would form because of the electron excitation caused by heat, which is similar to photocatalysis. O_2 can capture the excited electron to form ROS and prolong the lifetime of positive holes. In other words, the degradation of BPA would be slow without O_2, but it should keep a relatively stable degradation rate, since the constant input of heat. However, under N_2 atmosphere at 80 ℃, the TOC removal rate only increased from 37.5 % at 60 min to 42.1 % at 240 min (Fig. 3c), suggesting that the HC mechanism do not play the key role. SET and FRCAO mechanisms have a similar initial period[4], in which O_2 adsorbed on catalyst will harvest electron from organic with the catalyst as the bridge, resulting in the formation of $O_2^{\bullet-}$. Thus, in SET and FRCAO dominated processes, the O species of catalyst should have no obvious change, because the catalysts mainly play a role of electron transport. However, after being used under O_2 atmosphere, the ratios of O species changed a lot (Table 1, and Fig. 9c1 and c2), indicating that SET and FRCAO do not play the important role.

MVK mechanism includes two steps: 1) Pollutant oxidation by the lattice oxygen in the catalyst, and 2) re-oxidation of the catalyst by O_2[4]. There are three kinds of O species in PHM-$NiCo_2O_4$ (Table 1 and Fig. 9c1-c3), including lattice oxygen (O-metal), chemisorbed oxygen or hydroxyl-like group (O-O/OH) and adsorbed water (O-H_2O)[23,24,31]. According to a previous study[23], O-metal and O-O/OH can convert each other. Thus, O-metal and O-O/OH might have similar roles in BPA degradation. Being expressed by the atomic percent to total elements, the sum of O-metal and O-O/OH in as-prepared PHM-$NiCo_2O_4$, PHM-$NiCo_2O_4$ used under O_2 and PHM-$NiCo_2O_4$ used under N_2 are 30.5 %, 29.8 %, and 25.7 %, respectively (Table 1). Compared with as-prepared PHM-$NiCo_2O_4$, the sum of O-metal and O-O/OH of PHM-$NiCo_2O_4$ used under O_2 only lost 0.7 %, but for PHM-$NiCo_2O_4$ used under N_2, it lost about 4.8 % (Table 1). According to the MVK mechanism, the consumption of O-metal and O-O/OH would reduce Co^{3+} and Ni^{3+} to Co^{2+} and Ni^{2+}, respectively. The heavy loss of Co^{3+} (from 12.6 % to 2.7 %) under N_2 demonstrates that Co^{3+} has a crucial effect on the removal of BPA without O_2. For PHM-$NiCo_2O_4$ used under O_2, both the percentages of Co^{3+} (from 12.6 % to 10.3 %) and Ni^{3+} (from 5.0 % to 3.0 %) decreased (Table 1). The loss of Co^{3+} in PHM-$NiCo_2O_4$ used under O_2 is only 2.3 %, implying the re-oxidation of consumed Co^{3+} by O_2. Based on the above XPS analysis, the MVK mechanism is responsible for the formation of ROS.

Table 1
The percentage of specific chemical state of each element to total element, %.

		PHM-$NiCo_2O_4$	O_2-used, PHM-$NiCo_2O_4$	N_2-used, PHM-$NiCo_2O_4$
Ni	3 +	5.0	3.0	2.7
	2 +	7.3	6.0	6.3
Co	3 +	12.6	10.3	2.7
	2 +	4.6	4.8	12.2
O	O-metal	17.3	14.8	16.4
	O-O/OH	13.2	15.0	9.3
	O-H_2O	8.5	9.1	11.7
F	F-organic	7.3	9.0	14.5
	F-metal	5.5	0.3	1.0

Apart from O, Co and Ni species, there was also F species. F-organic species were not the active sites, because with a higher PTFE ratio (1:2), the PTFE-modified HM-$NiCo_2O_4$ had a much lower TOC removal rate than that of HM-$NiCo_2O_4$ (Fig. S4a). Besides, pure PTFE cannot degrade BPA (Fig. 3d), which also indicates that F-organic species were not active sites. After being used once under O_2 or N_2 atmosphere, the F species in the F-metal bond (F-metal species) almost disappeared (Fig. S12). Given that PHM-$NiCo_2O_4$ can be reused several times with high performance, the F-metal species did not play a crucial role in the catalysis.

3.3.3. Formation mechanism of ROS

The generation pathways of ROS are deduced from the foregoing analysis of the EPR and XPS results as Eqs. (1) - (8), where M stands for

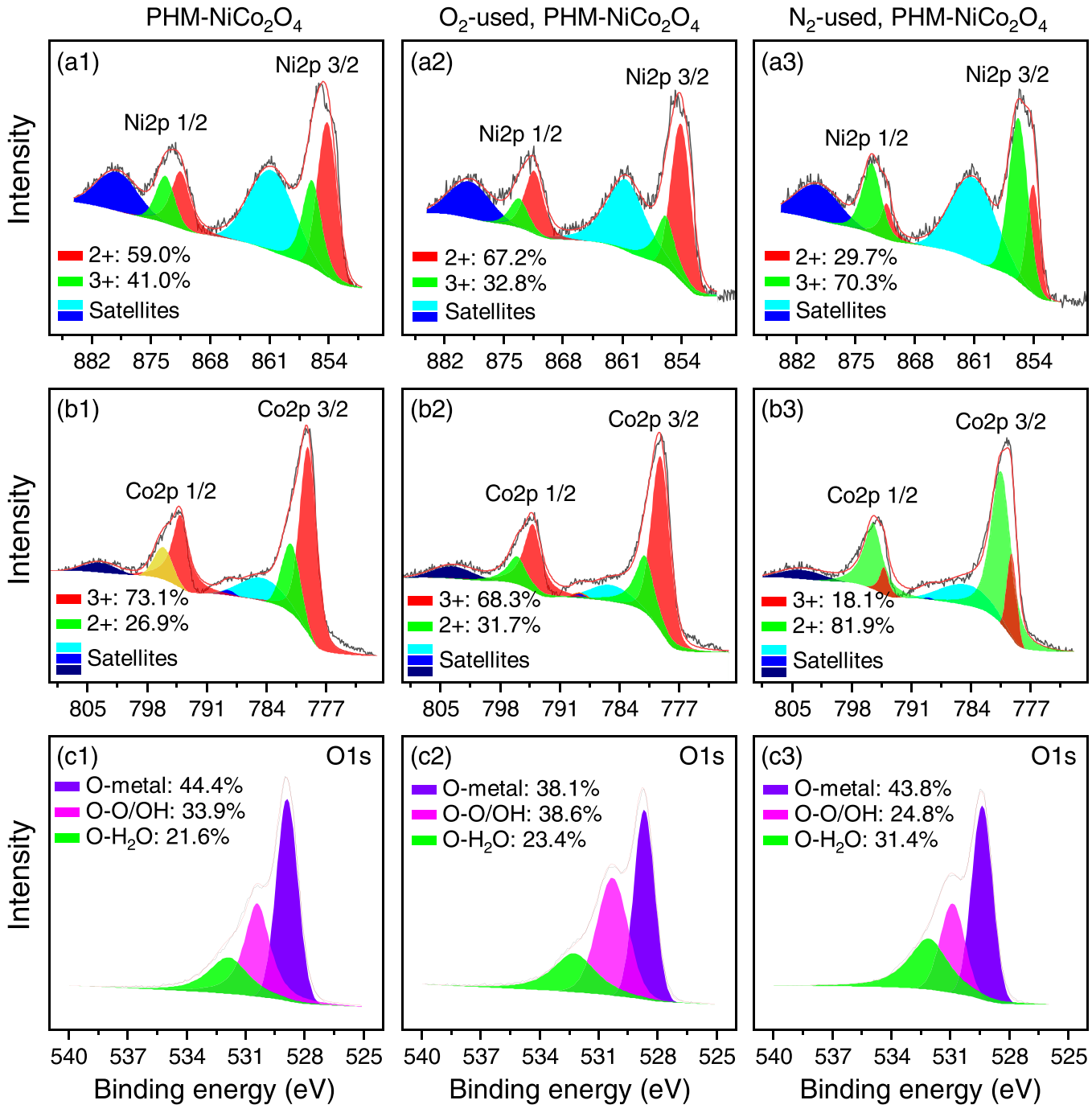

Fig. 9. Deconvolution spectra of Ni2p, Co2p and O1s of as-prepared PHM-$NiCo_2O_4$, used PHM-$NiCo_2O_4$ under O_2 and used PHM-$NiCo_2O_4$ under N_2, respectively (The percentage is the atomic percent of each chemical state to the element itself instead of total elements).

metal (Co or Ni) and V_O is for oxygen vacancy. The ERP signal of HO• was detected without BPA (Fig. 8a1), and just HO• was detected under N_2 (Fig. 8a3), suggesting that the formation of HO• does not need organics and O_2. Namely, HO• originates from the O species on PHM-$NiCo_2O_4$. After being used, the content of O-metal decreased (Table 1)· H_2O can participate in the formation of HO•[41]. Thus, Eqs. (1) and (2) are the possible ways of HO• generation. The formation of HO• would consume lattice oxygen and induce oxygen vacancy. The metals around oxygen vacancy have high ability to grab O_2 (Eq. (3))[42,43]. $O_2^{\bullet-}$ only appeared in the presence of O_2 (Fig. 8b1 and b2), demonstrating that the adsorbed O_2 takes part in the formation of $O_2^{\bullet-}$. There is study found that O_2 can directly grab one electron from oxygen vacancy to form $O_2^{\bullet-}$[44]. If O_2 is mainly used in this way, the consumed O-metal and O-O/OH cannot be compensated. Thus, $O_2^{\bullet-}$ might generate based on Eqs. (4) and (7), or based on Eqs. (5) and (7). Under O_2 atmosphere, the O-metal content of spent PHM-$NiCo_2O_4$ decreased, but the content of O-O/OH increased. Thus, Eqs. (5) and (7) are more likely to be the formation way of $O_2^{\bullet-}$. The re-oxidized PHM-$NiCo_2O_4$ can induce HO• formation through Eqs. (6) and (2) again, resulting in stronger EPR signal intensity under O_2 than that under N_2 (Fig. 8). The interaction between HO• and $O_2^{\bullet-}$ would lead to $^1O_2$ formation (Eq. (8))[45,46]. Previous studies had proved that HO•, $O_2^{\bullet-}$, and $^1O_2$ can degrade BPA (Eq. (9))[47–49].

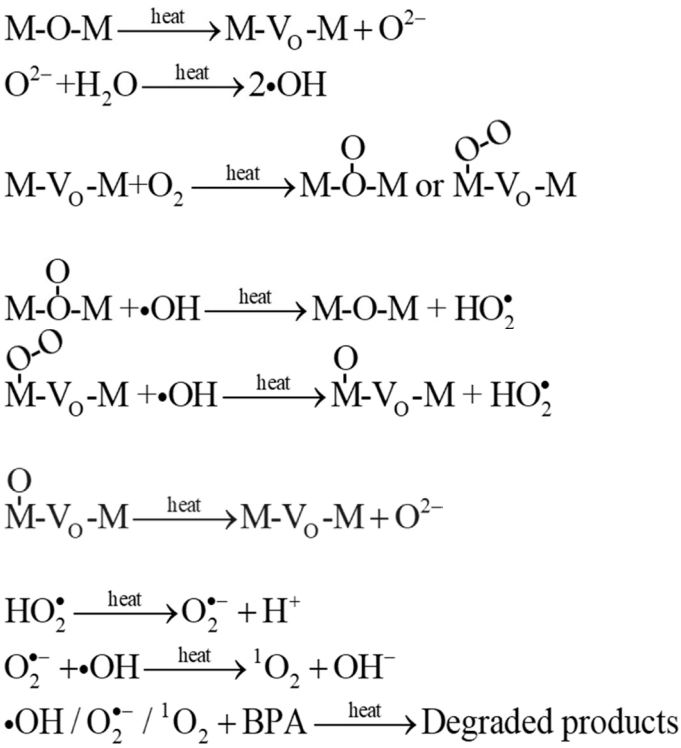

(1)

(2)

(3)

(4)

(5)

(6)

(7)

(8)

(9)

Quenching tests were further carried out to evaluate the role of HO•, $O_2^{\bullet-}$ and $^1O_2$. According to the second-order reaction rate constants (Table S3)[50,51], furfuryl alcohol (FFA) can effectively quench HO• and $^1O_2$, but not $O_2^{\bullet-}$. As shown in Fig. S13, FFA severely inhibited the removal of BPA (from nearly 100% to about 19%). Thus, HO• or $^1O_2$ is responsible for BPA removal. In systems with only $O_2^{\bullet-}$ formation, only 50 % of BPA (20 mg/L) is removed at 24 h[47]. In other words, $O_2^{\bullet-}$ indeed can degrade BPA, but the reaction rate is slow. The second order reaction rate constants of HO•/BPA and $^1O_2$/BPA are 1.8×10^{10} and 8.0×10^5 $M^{-1}s^{-1}$ at pH 7, respectively[40,51]. Thus, $^1O_2$ has a low reaction rate to degrade BPA as well. For instance, photoexcited rose bengal as a classical system for $^1O_2$ generation only can remove 10% of BPA (11.4 mg/L) within 60 min[49]. Spending the same time (60 min), in this study, more than 70 % of BPA (100 mg/L) was removed in the absence of NaCl (Fig. S13). Thus, $^1O_2$ should not be the vital ROS in this study. However, methanol (MeOH) and tertiary butanol (TBA) as the quenchers of HO• had limited inhibition in BPA removal. Noting that the boiling point of MeOH, TBA and FFA are 65, 83 and 170 ℃, respectively, thus, the low inhibition degree of MeOH and TBA should be owing to their volatilization. Based on the second order reaction rate constants (Table S3), MeOH should has stronger ability to quench HO• than TBA, but in this study, TBA resulted in more severe suppression. This is due to the higher boiling point of TBA than MeOH. In short, HO• should play the critical role, but $O_2^{\bullet-}$ and $^1O_2$ also participate in BPA removal.

4. Conclusion

Aiming to enhance the catalytic performance of HM-$NiCo_2O_4$ in AP-CWAO for treating high-salt organic wastewater, PTFE modification was used to enhance the O_2 transfer and salts resistibility of HM-$NiCo_2O_4$. PHM-$NiCo_2O_4$ performed better in BPA removal than HM-$NiCo_2O_4$, and this superiority was even more pronounced in the 10 g/L NaCl solution. Due to the lipophobicity of PTFE, it has no ability to adsorb BPA, and PTFE modification enhanced the degradation instead of adsorption of BPA. DFT calculations and MD simulations show that PTFE modification indeed can enhance O_2 transfer and salts resistibility of HM-$NiCo_2O_4$. PHM-$NiCo_2O_4$ has good stability, and after being used four times, the TOC removal rate only lost about 8 %. Cl^- and Mg^{2+} had low inhibition on mineralization of BPA, but it is relative sever by SO_4^{2-} and Ca^{2+}. BPA was degraded by HO•, $O_2^{\bullet-}$ and $^1O_2$, and these ROS formed based on Mars-van Krevelen mechanism.

Declaration of Competing Interest

The authors declare that they have no known competing financial interests or personal relationships that could have appeared to influence the work reported in this paper.

Data availability

No data was used for the research described in the article.

Acknowledgments

The authors are grateful for the financial support from the National Science Fund for Distinguished Young Scholars (Grant No. 21925801), the Fund for Innovative Research Group of National Natural Science Foundation of China (Grant No. 51721006), the National Natural Science Foundation of China (Grant No. 22178222), and Guangdong Basic and Applied Basic Research Foundation (Grant No. 2021A1515010540).

Appendix A. Supporting information

Supplementary data associated with this article can be found in the online version at doi:10.1016/j.apcatb.2023.122786.

References

[1] F. Luck, A review of industrial catalytic wet air oxidation processes, Catal. Today 27 (1996) 195–202.

[2] H. Tan, S. Wang, J. Wang, F. Song, X. Sun, R. Zhao, Y. Zhang, H. Cui, High-efficiency catalytic wet air oxidation of high salinity phenolic wastewater under atmospheric pressure in molten salt hydrate media, N. J. Chem. 45 (2021) 2167–2174.

[3] Y. Bao, W.J. Lee, P. Wang, J. Xing, Y.N. Liang, T.-T. Lim, X. Hu, A novel molybdenum-based nanocrystal decorated ceramic membrane for organics degradation via catalytic wet air oxidation (CWAO) at ambient conditions, Catal. Today 364 (2021) 276–284.

[4] H. Chen, J. Ku, L. Wang, Thermal catalysis under dark ambient conditions in environmental remediation: fundamental principles, development, and challenges, Chin. J. Catal. 40 (2019) 1117–1134.

[5] Z. Zhang, Y. Gao, Q. Wang, Fabrication, activity and mechanism studies of transition metal molybdate/molybdenum trioxide hybrids as novel CWAO catalysts, Sep. Purif. Technol. 191 (2018) 354–363.

[6] W. Sun, H. Wei, L. yang An, C. Jin, H. Wu, Z.-a Xiong, C. Pu, C. Sun, Oxygen vacancy mediated $La_{1-x}Ce_xFeO_3$-δ perovskite oxides as efficient catalysts for CWAO of acrylic acid by A-site Ce doping, Appl. Catal. B 245 (2019) 20–28.

[7] S. Yang, M. Besson, C. Descorme, Catalytic wet air oxidation of succinic acid over Ru and Pt catalysts supported on $Ce_xZr_{1-x}O_2$ mixed oxides, Appl. Catal. B 165 (2015) 1–9.

[8] T.J. Makatsa, J. Baloyi, T. Ntho, C.M. Masuku, Catalytic wet air oxidation of phenol: Review of the reaction mechanism, kinetics, and CFD modeling, Crit. Rev. Environ. Sci. Technol. 51 (2021) 1891–1923.

[9] S.J. Baloyi, J.A. Moma, Catalytic wet air oxidation of phenol by cordierite honeycomb washcoated with Al/Zr pillared bentonite in a plug flow reactor, J. Environ. Chem. Eng. 8 (2020), 104186.

[10] J.O. Valderrama, R.A. Campusano, L.A. Forero, A new generalized Henry-Setschenow equation for predicting the solubility of air gases (oxygen, nitrogen and argon) in seawater and saline solutions, J. Mol. Liq. 222 (2016) 1218–1227.

[11] J. Wang, S. Wang, Effect of inorganic anions on the performance of advanced oxidation processes for degradation of organic contaminants, Chem. Eng. J. 411 (2021), 128392.

[12] S. Wang, X. Li, Z. Wan, Y. Chen, J. Tan, M. Pan, Effect of hydrophobic additive on oxygen transport in catalyst layer of proton exchange membrane fuel cells, J. Power Sources 379 (2018) 338–343.

[13] W.-W. Tian, J.-T. Ren, X.-W. Lv, Z.-Y. Yuan, A "gas-breathing" integrated air diffusion electrode design with improved oxygen utilization efficiency for high-performance Zn-air batteries, Chem. Eng. J. 431 (2022), 133210.

[14] D. Wakerley, S. Lamaison, F. Ozanam, N. Menguy, D. Mercier, P. Marcus, M. Fontecave, V. Mougel, Bio-inspired hydrophobicity promotes CO_2 reduction on a Cu surface, Nat. Mater. 18 (2019) 1222–1227.

[15] Y. Yang, H. Zhao, Z. Yin, J. Zhao, X. Yin, N. Li, D. Yin, Y. Li, B. Lei, Y. Du, W. Que, A general salt-resistant hydrophilic/hydrophobic nanoporous double layer design for efficient and stable solar water evaporation distillation, Mater. Horiz. 5 (2018) 1143–1150.

[16] W.-m Zhang, J. Yan, Q. Su, J. Han, J.-f Gao, Hydrophobic and porous carbon nanofiber membrane for high performance solar-driven interfacial evaporation with excellent salt resistance, J. Colloid Interface Sci. 612 (2022) 66–75.

[17] X. Chen, C. Dai, T. Zhang, P. Xu, W. Ke, J. Wu, M. Qiu, K. Fu, Y. Fan, Efficient construction of a robust PTFE/Al_2O_3 hydrophobic membrane for effective oil purification, Chem. Eng. J. 435 (2022), 134972.

[18] J. Lin, S. Yan, C. Zhang, Q. Hu, Z. Cheng, Hydrophobic electrode design for CO_2 electroreduction in a microchannel reactor, ACS Appl. Mater. Interfaces 14 (2022) 8623–8632.

[19] A. Bezuidenhoudt, P.W. Sonnendecker, P.L. Crouse, Temperature and pressure effects on the product distribution of PTFE pyrolysis by means of qualitative, in-line FTIR analysis, Polym. Degrad. Stab. 142 (2017) 79–88.

[20] Y. Wang, Y. Xu, S. Dong, P. Wang, W. Chen, Z. Lu, D. Ye, B. Pan, D. Wu, C. D. Vecitis, G. Gao, Ultrasonic activation of inert poly(tetrafluoroethylene) enables piezocatalytic generation of reactive oxygen species, Nat. Commun. 12 (2021) 3508.

[21] J. Li, Y. Qiao, T. Pan, K. Zhong, J. Wen, S. Wu, F. Su, Y. Tian, Amphiphilic fluorine-containing block copolymers as carriers for hydrophobic pttfpp for dissolved oxygen sensing, cell respiration monitoring and in vivo hypoxia imaging with high quantum efficiency and long lifetime, Sensors 18 (2018).

[22] J.G. Riess, Understanding the fundamentals of perfluorocarbons and perfluorocarbon emulsions relevant to in vivo oxygen delivery, Artif. Cells Nanomed. Biotechnol. 33 (2005) 47–63.

[23] Q. Jing, H. Li, Hierarchical nickel cobalt oxide spinel microspheres catalyze mineralization of humic substances during wet air oxidation at atmospheric pressure, Appl. Catal. B 256 (2019), 117858.

[24] Q. Liu, L. Xie, J. Liang, Y. Ren, Y. Wang, L. Zhang, L. Yue, T. Li, Y. Luo, N. Li, B. Tang, Y. Liu, S. Gao, A.A. Alshehri, I. Shakir, P.O. Agboola, Q. Kong, Q. Wang, D. Ma, X. Sun, Ambient ammonia synthesis via electrochemical reduction of nitrate enabled by $NiCo_2O_4$ nanowire array, Small 18 (2022), 2106961.

[25] X.Q. Zhang, Y.C. Zhao, C.G. Wang, X. Li, J.D. Liu, G.H. Yue, Z.D. Zhou, Facile synthesis of hollow urchin-like $NiCo_2O_4$ microspheres for high-performance sodium-ion batteries, , J. Mater. Sci. 51 (2016) 9296–9305.

[26] N. Panigrahy, A. Priyadarshini, M.M. Sahoo, A.K. Verma, A. Daverey, N.K. Sahoo, A comprehensive review on eco-toxicity and biodegradation of phenolics: recent progress and future outlook, Environ. Technol. Innov. 27 (2022), 102423.

[27] H. Zhang, Z. Ling, J. Ma, Y. Nie, Biodegradability enhancement of phenolic wastewater using hydrothermal pretreatment, Bioresour. Technol. 367 (2023), 128199.

[28] F. Neese, Software update: The ORCA program system—Version 5.0, 12 (2022) e1606.

[29] T. Lu, F.W. Chen, Multiwfn: a multifunctional wavefunction analyzer, J. Comput. Chem. 33 (2012) 580–592.

[30] A.P. Thompson, H.M. Aktulga, R. Berger, D.S. Bolintineanu, W.M. Brown, P. S. Crozier, P.J. in 't Veld, A. Kohlmeyer, S.G. Moore, T.D. Nguyen, R. Shan, M. J. Stevens, J. Tranchida, C. Trott, S.J. Plimpton, LAMMPS – a flexible simulation tool for particle-based materials modeling at the atomic, meso, and continuum scales, Comput. Phys. Commun. 271 (2022), 108171.

[31] X.-Y. Yu, X.-Z. Yao, T. Luo, Y. Jia, J.-H. Liu, X.-J. Huang, Facile synthesis of Urchin-like NiCo2O4 hollow microspheres with enhanced electrochemical properties in energy and environmentally related applications, ACS Appl. Mater. Interfaces 6 (2014) 3689–3695.

[32] K.S.W. Sing, Reporting physisorption data for gas/solid systems with special reference to the determination of surface area and porosity (Recommendations 1984), Pure Appl. Chem. 57 (1985) 603–619.

[33] M. Thommes, K. Kaneko, A.V. Neimark, J.P. Olivier, F. Rodriguez-Reinoso, J. Rouquerol, K.S.W. Sing, Physisorption of gases, with special reference to the evaluation of surface area and pore size distribution (IUPAC Technical Report), Pure Appl. Chem. 87 (2015) 1051–1069.

[34] X. Yu, C. Wei, H. Wu, Z. Jiang, R. Xu, Improvement of biodegradability for coking wastewater by selective adsorption of hydrophobic organic pollutants, Sep. Purif. Technol. 151 (2015) 23–30.

[35] N.G. Camparotto, Td.F. Neves, V.R. Mastelaro, P. Prediger, Hydrophobization of aerogels based on chitosan, nanocellulose and tannic acid: improvements on the aerogel features and the adsorption of contaminants in water, Environ. Res 220 (2023), 115197.

[36] Ss Ai, X. Guo, L. Zhao, D. Yang, Hm Ding, Zeolitic imidazolate framework-supported Prussian blue analogues as an efficient Fenton-like catalyst for activation of peroxymonosulfate, Colloid Surf. A-Physicochem. Eng. Asp. 581 (2019), 123796.

[37] J. Wang, S. Wang, Activation of persulfate (PS) and peroxymonosulfate (PMS) and application for the degradation of emerging contaminants, Chem. Eng. J. 334 (2018) 1502–1517.

[38] F. Ghanbari, M. Moradi, Application of peroxymonosulfate and its activation methods for degradation of environmental organic pollutants: review, Chem. Eng. J. 310 (2017) 41–62.

[39] Q. Yang, Y.H. Ma, F. Chen, F.B. Yao, J. Sun, S.N. Wang, K.X. Yi, L.H. Hou, X.M. Li, D.B. Wang, Recent advances in photo-activated sulfate radical-advanced oxidation process (SR-AOP) for refractory organic pollutants removal in water, Chem. Eng. J. 378 (2019), 122149.

[40] Z. Lin, W. Qin, L. Sun, X. Yuan, D. Xia, Kinetics and mechanism of sulfate radical- and hydroxyl radical-induced degradation of Bisphenol A in VUV/UV/peroxymonosulfate system, J. Water Process. Eng. 38 (2020), 101636.

[41] Y. Xu, H. Shao, F. Ge, Y. Liu, Novel-structured Mo-Cu-Fe-O composite for catalytic air oxidation of dye-containing wastewater under ambient temperature and pressure, Chin. J. Catal. 38 (2017) 1719–1725.

[42] J. Yang, S. Hu, Y. Fang, S. Hoang, L. Li, W. Yang, Z. Liang, J. Wu, J. Hu, W. Xiao, C. Pan, Z. Luo, J. Ding, L. Zhang, Y. Guo, Oxygen vacancy promoted O2 activation over perovskite oxide for low-temperature CO oxidation, ACS Catal. 9 (2019) 9751–9763.

[43] D. Yun, Y. Wang, J.E. Herrera, Ethanol partial oxidation over VOx/TiO2 catalysts: the role of titania surface oxygen on vanadia reoxidation in the Mars–van Krevelen mechanism, ACS Catal. 8 (2018) 4681–4693.

[44] L. Wu, Z. Sun, Y. Zhen, S. Zhu, C. Yang, J. Lu, Y. Tian, D. Zhong, J. Ma, Oxygen vacancy-induced nonradical degradation of organics: critical trigger of oxygen (O2) in the Fe–Co LDH/peroxymonosulfate system, Environ. Sci. Technol. 55 (2021) 15400–15411.

[45] Y. Wen, C.-H. Huang, D.C. Ashley, D. Meyerstein, D.D. Dionysiou, V.K. Sharma, X. Ma, Visible light-induced catalyst-free activation of peroxydisulfate: pollutant-dependent production of reactive species, Environ. Sci. Technol. 56 (2022) 2626–2636.

[46] F. Sun, T. Chen, H. Liu, X. Zou, P. Zhai, Z. Chu, D. Shu, H. Wang, D. Chen, The pH-dependent degradation of sulfadiazine using natural siderite activating PDS: the role of singlet oxygen, Sci. Total Environ. 784 (2021), 147117.

[47] H. Javed, J. Metz, T.C. Eraslan, J. Mathieu, B. Wang, G. Wu, A.-L. Tsai, M.S. Wong, P.J.J. Alvarez, Discerning the relevance of superoxide in PFOA degradation, Environ. Sci. Technol. Lett. 7 (2020) 653–658.

[48] Z.-H. Xie, C.-S. He, H.-Y. Zhou, L.-L. Li, Y. Liu, Y. Du, W. Liu, Y. Mu, B. Lai, Effects of molecular structure on organic contaminants' degradation efficiency and dominant ROS in the advanced oxidation process with multiple ROS, Environ. Sci. Technol. 56 (2022) 8784–8795.

[49] E.-T. Yun, J.H. Lee, J. Kim, H.-D. Park, J. Lee, Identifying the nonradical mechanism in the peroxymonosulfate activation process: singlet oxygenation versus mediated electron transfer, Environ. Sci. Technol. 52 (2018) 7032–7042.

[50] L. Gao, Y. Guo, J. Zhan, G. Yu, Y. Wang, Assessment of the validity of the quenching method for evaluating the role of reactive species in pollutant abatement during the persulfate-based process, Water Res. 221 (2022), 118730.

[51] J. Lee, U. von Gunten, J.H. Kim, Persulfate-based advanced oxidation: critical assessment of opportunities and roadblocks, Environ. Sci. Technol. 54 (2020) 3064–3081.